Growth and Transport Properties of [Rare Earth]TiO3/SrTiO3 Interfaces

Lebedev, N.

5

On the superconducting-insulator transition in disordered oxide interfaces

The Superconductor-Insulator transition (SIT) in the two-dimensional electron gas at the $LaAlO_3/SrTiO_3$ interface has attracted attention due to the possibility to tune it with both gate voltage and magnetic field. Moreover, it has been argued that magnetic ordering coexists with superconductivity in this system, and in particular the observation of hysteretic magnetoresistance has been interpreted to be one of the manifestations of that phenomenon. In this work, we have studied two different disordered oxide interfaces, namely amorphous $LaTiO_3/SrTiO_3$ and intermixed $LaAlO_3/GdTiO_3/SrTiO_3$. We observed that both systems show the behavior of granular superconductors and also a gate-tunable SIT. Moreover, both systems show hysteretic magnetoresistance. However, we will argue that such hysteresis arises from the granular superconducting state, and not from magnetic order.

5.1. Introduction

The occurrence of superconductivity in the two-dimensional electron gas at the interface between $SrTiO_3$(STO) and another oxide with a crystalline [3, 4, 57, 140] or amorphous [226] structure is a well-established fact. The superconducting state can be driven into a weakly localized metallic state by applying a gate voltage [4] or a magnetic field [73, 169]. This is usually called a Superconductor-Insulator transition (SIT) since the weakly localised state is often referred to as insulating. The first study of the nature of the SIT with gate voltage in $LaAlO_3$/STO (LAO/STO) [4] considered the behavior of the critical temperature (actually the Berezinskii-Kosterlitz-Thouless temperature T_{BKT}) as function of back gate voltage, using the concept of a quantum critical point. A scaling theory analysis gave a product of the critical exponents $\nu z = 2/3$, indicating a fermionic scenario, while at the same time the critical resistance at the transition was close to 6.5 kOhm, which is expected for a dirty boson scenario [70–72]. The difference between two scenarios is the behavior of Cooper pairs across the transition. In the fermionic scenario, Cooper pairs are destroyed on the nonsuperconducting side [71]; in the dirty boson scenario, they survive in mesoscopic puddles [70–72]. Subsequent work by Biscaras *et al.* [169] on the magnetic-field-driven SIT in $LaTiO_3$/STO (LTO/STO) showed multiple quantum critical points, but basically concluded for a bosonic scenario. That scenario was also supported by a study of the magnetic-field-driven SIT in LAO/STO, but the product of the critical exponents was $\nu z = 7/3$, which corresponds to quantum percolation in insulating state [73], *i.e.*, Cooper pairs tunnel between localized superconducting islands [72]. On the whole, a dirty-boson scenario involving a (dirty boson) inhomogeneous superconducting state is an accepted picture for the SIT at oxide interfaces.

Another and somewhat puzzling aspect comes from the issue of the possible existence of magnetism. Signatures of magnetism in the superconducting state were found by SQUID microscopy [6] and magnetic torque experiments [7]. At the same time, the transport measurements demonstrated hysteretic magnetoresistance in superconducting LAO/STO [8, 74, 79, 80], which then also were interpreted as evidence of the coexistence of superconductivity and magnetism. Moreover, superconductivity and hysteresis also were observed in the LAO/STO interface delta-doped by ferromagnetic $EuTiO_3$ (ETO) [132]. The hysteresis was found at gate voltages where also an Anomalous Hall Effect (AHE) was observed, as a hallmark for magnetism. Neither hysteresis nor AHE was present at gate voltages which invoked the insulating Kondo-like state, either above or below T_c.

In this work we present a study of SIT in two disordered oxide interface

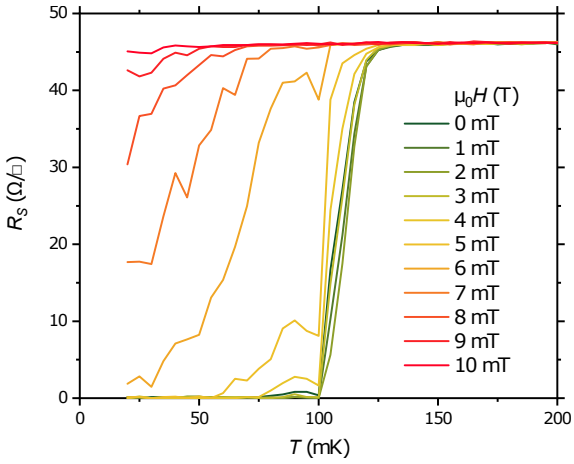

Figure 5.1: Sheet resistance R_S as function of temperature T at different magnetic fields applied out of the sample plane, as indicated. The sample is a-LTO/STO.

systems, namely amorphous LTO/STO (a-LTO/STO) and intermixed crystalline $LaAlO_3/GdTiO_3/SrTiO_3$. Details of sample growth, in both cases, have been described in the Chapters 3 and 4. Previously, we found for a-LTO/STO, that the LTO layer tends to amorphize, and these heterostructures show gate tunable superconductivity in wide voltage range with strong indications of large spatial non-uniformities(see Chapter 4). The second system suffered from strong intermixing, and layers are rather $La_{1-x}Gd_xAlO_3/Gd_{1-y}La_yTi_{1-z}Al_zO_3$/STO (LGAO/GLTAO/STO). This system exhibits an Anomalous Hall effect (AHE) at 3 K without hysteresis and, as we found, without becoming ferromagnetic. The point to make here is that in both cases a gate-tunable SIT is present, and hysteresis is found, but this appears to be due to the granular superconducting state of the system and not to any magnetism. In a-LTO/STO, to be presented first, we find a re-entrant superconducting transition due to large scale inhomogeneities. In LGAO/GLTAO/STO we find a temperature dependence on the insulating side that usually observed in other systems with disordered SIT, but so far has not been reported in LAO/STO.

The samples were measured in a Van der Pauw geometry using a dilution refrigerator (a Triton from Oxford Instruments)[1]. The gate voltage was always swept from positive to negative, with a starting point at 100 V.

[1]The transport measurements were performed by Dr. Martin Stehno at the University of Twente

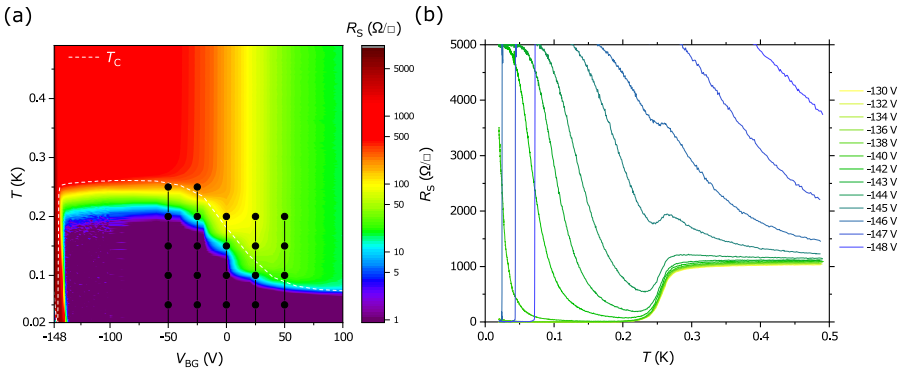

Figure 5.2: (a) Resistance map of a-LTO/STO with the color scale indicating the magnitude of the sheet resistance R_S. Black dots represent points where the field dependence of the *MR* was measured (see Fig. 5.3). Black vertical lines are guides to the eye. The white dashed line represents T_c determined as the temperature at 50% drop of the sheet resistance. (b) $R_S(T)$ at different gate voltages for LTO/STO near the Superconductor-Insulator transition (SIT).

5

5.2. Study of a-LTO/STO

5.2.1. Results

We start with the temperature dependence of the sheet resistance in different fields (Fig. 5.1) oriented in the out-of-plane direction. Compared to previous measurements on LAO/STO [3, 57], much smaller fields are required to suppress the superconductivity in a-LTO/STO. At low fields (< 5 mT), the sample shows a steplike drop in resistance at high temperatures and a shoulder feature at low temperatures. The initial drop is almost unaffected by the applied field in contrast to the shoulder. This behavior, and the low fields involved, make clear that we do not observe a conventional critical field H_{c2}. The response rather resembles that of granular cuprate superconductors [245–247], granular NbN films [248] and proximity coupled superconducting arrays [249, 250]. The drop corresponds to developing superconductivity in granules, and the shoulder is due to transitions in the weak links between granules.

To investigate the superconductivity further, we applied a back gate voltage V_{BG}. Fig. 5.2a shows the color-coded sheet resistance R_S as function of V_{BG} and temperature. Superconductivity with a low T_c persists up to 100 V, but the values usually found in these systems, around 200 mK, are found for negative V_{BG}. The step-like features in Fig. 5.2a are an artifact due to large (20 V) spacing used to measure

curves above -60 V. The shows a sharp SIT at large negative gate voltages. Although usually less sharp [4, 59], some groups have observed such a sharp transition [60]. In Fig. 5.2b we show the temperature dependence of R_S for different V_{BG} at the onset of the SIT. In the region intermediate between superconducting transitions and a monotonous resistance rise, we find that R_S goes through a minimum. A further decrease of the gate voltage appears to lead to re-entrance, which may be due to a very inhomogeneous superconducting state in a-LTO/STO as we observed it previously (see Chapter 4); or, more likely, to an artefact when the sample resistance becomes larger than the amplifier impedance.

Besides the SIT, we observe hysteresis in the magnetic field dependence of R_S below T_c (with the field again pointing out of the plane). Fig. 5.3 shows that such hysteresis becomes significant below the 50% resistance decrease line in the superconducting transition, indicating the correlation with the superconducting state. The sweep rate for this measurement was 0.833 mT/s. The butterfly shape of the hysteresis is similar to the earlier reports in LAO/STO [8, 74]. This shape is peculiar because the hysteretic loops open up before field passes zero during the reverse sweep. Such behavior is not at all typical for ferromagnet, where the opposite would be expected, but often can be seen in granular HTC materials due to flux dynamics and trapping [246, 247, 251–257]. The fields of the dip features do not change significantly with temperature.

Following up on the thought of flux dynamics, we next consider the sweep-rate dependence of hysteretic magnetoresistance (*MR*) in more detail. The *MR* at V_{BG} = 30 V and T = 25 mK at different sweep rates between roughly 0.8 mT/s and 0.03 mT/s are presented in Fig. 5.4a for both directions of the field sweep, and, for clarity, in Fig. 5.4b for a single (negative to positive) direction. We see various dips develop. In the down sweep, an increasingly large dip (with increasing sweep rate) develops on the positive field side before crossing zero field, followed by a smaller dip in the negative quadrant, while in the sweep up, the situation is reversed. Note that dip on decreasing sweep has not been observed by Mehta *et al.* [74]. Moreover, we found that the sweep rate dependence of the magnitude of big and small dips are different. To describe the behavior we use the ratio of the dip resistance R^{dip} normalized by its highest value $R^{dip}_{0.8}$, at the fastest sweep rate of 0.83 mT/s. We find that the ratio can be fitted by a power law.

$$R^{dip}/R^{dip}_{0.8} = A(\mu_0 \dot{H})^p, \tag{5.1}$$

where $\mu_0 \dot{H}$ is sweep rate, and A and p are fitting parameters. The first forward dip is better fitted with equation

$$R^{dip}/R^{dip}_{0.8} = 1 + Ce^{-\mu_0 \dot{H}/R}, \tag{5.2}$$

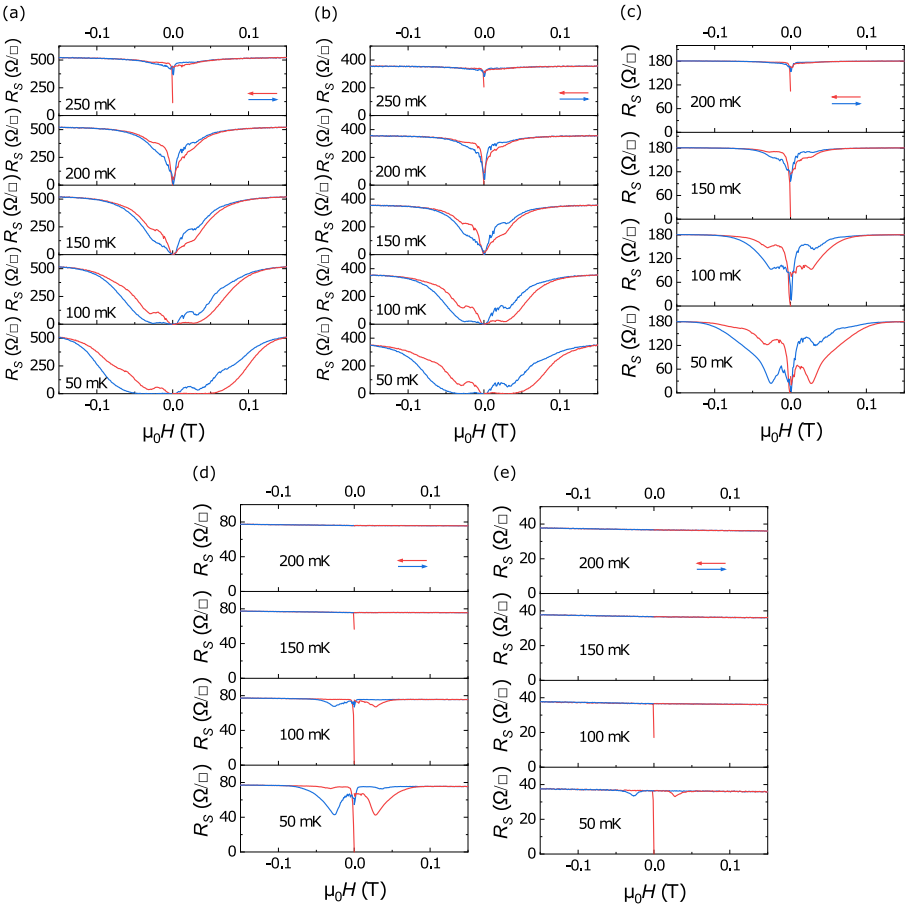

Figure 5.3: Magnetoresistance hysteresis in a-LTO/STO at various temperatures and at the following back gate voltage: (a) -50, (b) -25, (c) 0, (d) 25 and (e) 50 V.

where C and R are fitting parameters. The fit of the data with Eq. 5.1 and 5.2 is shown in Fig. 5.4c.

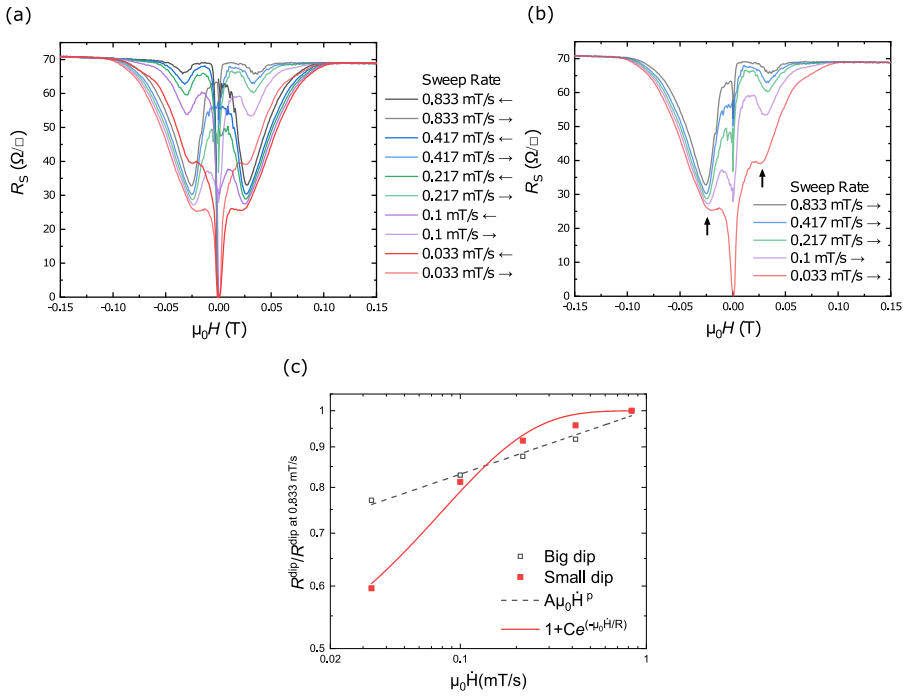

Figure 5.4: (a) Magnetoresistance in a-LTO/STO at different magnetic field sweep rates for a gate voltage of 30 V at 25 mK. (b) The same data, but only one sweep direction is shown. The left-hand arrow shows the position of the big dip, the right-hand arrow that of the small dip. (c) Sweep rate dependence of normalized dips in a-LTO/STO and corresponding fits. Note the log scale on the horizontal axis.

5.2.2. Discussion

Hysteretic *MR* was studied in various STO-based structures, and to draw conclusions with respect to the effects of superconductivity and, possibly, magnetism, it is important to consider the temperature where the hysteresis disappears, and the dependence on sweep rate. In LAO/STO nanowires [80], hysteris disappears well above T_c and is sweep rate independent; similarly, in LAO/$EuTiO_3$/STO [132] hysteresis is observed above T_c. Also in GTO/STO, GTO/STO/GTO [174], and in La:STO [174] structures, hysteresis was found above T_c, but presence or absence of sweep rate dependence was not reported. In these systems, magnetism probably plays a role, although effects of heating while sweeping the field, and subsequent

hysteresis, cannot be always ruled out [81, 82, 258]. In LAO/STO itself, the situation is still no clear. Dikin *et al.* reported the onset of hysteresis in out-of-plane *MR* with an onset at T_c, but in the insulating phase also hysteresis at higher temperatures [8]. In later work, they also reported a sweep rate dependence of the hysteresis [74]. The results were interpreted as the co-existence of magnetism and superconductivity. Our results (hysteresis and a sweep rate dependence below T_c would indicate that no magnetism needs to be assumed on the superconducting side, but can exist on the insulating side of the doping phase diagram. In Ref. [79], hysteretic in-plane magnetoresistance was found to develop below T_c, which was explained by the existence of ferromagnetic dipoles outside the 2DEG.

In our case, as we know from TEM studies (see Section 4.3.1, a-LTO/STO is amorphous. Redox reactions in a-LTO/STO cannot be well controlled and can easily lead to the development of large inhomogeneous regions leading to percolation behavior(see Chapter 4). Therefore, other mechanisms may lead to hysteretic *MR*. In particular flux trapping in granular superconductors can give rise to the hysteresis of the critical current [246, 253, 256, 257, 259], which leads to hysteretic magnetoresistace [247, 251, 252, 254, 255]. Qualitatively it can be described by a two-level model, where the sample is represented by superconducting grains and a weak link network [257, 260]. In such systems, the magnetic flux can be trapped in grains, with shielding current flowing through the network of weak links [257]. Applying this to our case, the initial field increase leads to penetration of the magnetic field through the weak links, to the destruction of the weakest Josephson junctions, and, therefore, to an increase of resistance. The non-monotonous dependence of resistance in increasing branch of the field sweep dependence can be a result of complex rearrangements of weak links or the pinning of Josephson vortices in intergranular media. At some magnetic field, the magnetic flux will penetrate the grains and produce a current, which leads to diamagnetic contribution to the magnetization. When the magnetic field decreases, this current is reversed and produces a paramagnetic contribution to the magnetization, reducing the average field within junction in the Josephson junction network. The field at which the dip on the reverse curve reaches its minimum is the point where there is a maximum cancellation between the applied field and trapped flux. With the further reduction of the magnetic field to zero, most of the flux escapes from the weak link network, and magnetic flux from grains suppresses the maximum of critical current. In reversing the magnetic field, the trapped flux will be aligned with the applied field suppressing critical current further. Moreover, this will not be a two-level system; the strength of the Josephson coupling can vary across samples producing more complex magnetization behavior of grains and intergrain media [255, 257]. This and complex pinning mechanism are the most likely reasons why we do not observe the expected dependence $R \propto ln(\dot{H})$ [261–264].

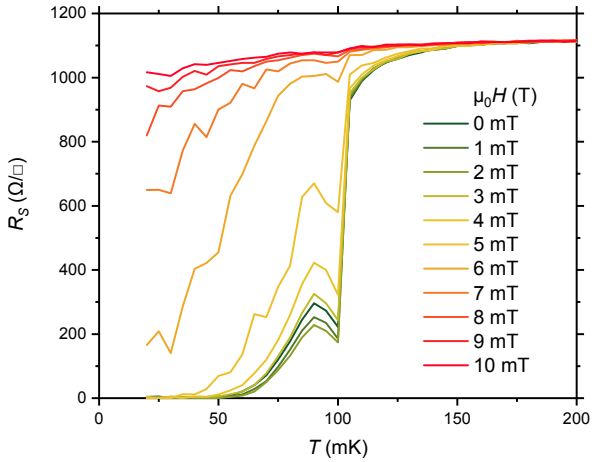

Figure 5.5: The sheet resistance $R_S(T)$ at different out-of-plane magnetic fields for LGAO/GLATO/STO.

5.3. Study of LGAO/GLATO/STO

5.3.1. Results

The temperature dependence for different magnetic field of LGAO/GLATO/STO is shown in Fig. 5.5 and, like a-LTO/STO, exhibits small critical fields, as well as an initial drop in resistance at high temperatures followed by a shoulder feature at low temperatures. The drop and shoulder behave qualitatively similar to a-LTO/STO and point again to the existence of granular superconductivity. However, backgate experiments find quite different behavior for the SIT in the sense that it occurs at a much smaller negative gate voltage, around -5 V to -10 V, as shown in Fig. 5.6a. From the temperature dependence of the sheet resistance in Fig. 5.6b it can be seen that there are three distinct regimes, superconducting, metallic, and insulating. The 50% line (resistance has dropped to 50% of the normal state value) of T_c in Fig. 5.3a has a sharp decrease near SIT, indicating insensitivity to small features in transition.

In this case, to study the superconducting state, we measured $I(V)$ curves at different temperatures and gate voltages. Measurements at 40 V, 20 V, 5 V and 0 V are presented in Fig. 5.7a-d. The $I(V)$ curves, presented in log-log fashion, show multiple steps, which indicates inhomogeneous superconductivity in our sample similar to LAO/STO [3]. In various sections of the $I(V)$ curves we observe power-

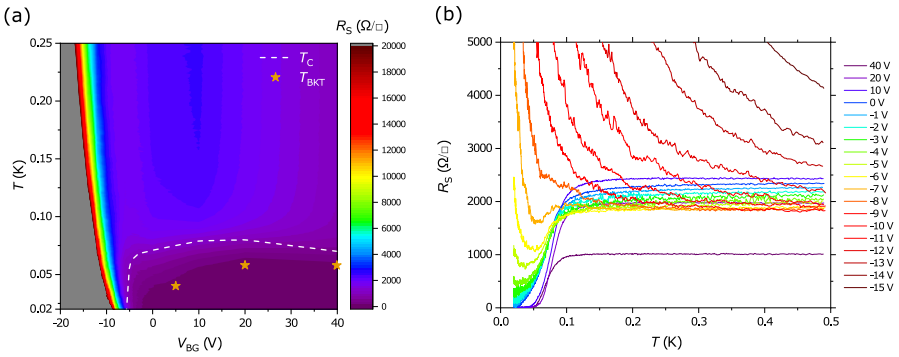

Figure 5.6: (a)-(b) Resistance map of LGAO/GLTAO/STO with the color scale indicating the magnitude of the sheet resistance R_S. Stars and dashed line represent T_{BKT} determined from the $I(V)$ characteristics and T_c determined as the temperature at 50 % drop of the sheet resistance. (b) $R_S(T)$ at different gate voltages for LGAO/GLTAO/STO.

law dependences and from that determined the Berezinskii–Kosterlitz–Thouless transition temperature (T_{BKT}) using the $V \sim I^3$ criterion [3]. It means we find the temperature where that power law holds, as indicated by the dashed lines in the Figure. Note that the same power 3 holds for homogeneous systems and for proximity-coupled superconducting arrays [249]. The values for T_{BKT} do not follow the 50% line, and in particular drop below the lowest measured temperature at 0 V, close to when $R(T)$ start to exhibit finite resistance. Furthermore, T_{BKT} is significantly below the 50% line, indicating again that T_c is not that of a homogeneous system but rather the signature of the formation of weak link network like in granular superconductor system [248], similar to Josephson Junction arrays [249, 250]. Recently, it was argued that $V \sim I^3$ scaling in STO-based interfaces can arise due to puddle-like inhomogeneities [265] where the network is built from puddles with different strength rather than connected by weak links, but for our LGAO/GLTAO/STO sample a two-level model based on the superconducting granules and weak links network, where $V \sim I^3$ is signature of superconductivity in weak links [257, 266] describe data better.

The temperature dependence of the resistance in the insulating phase can be described by Efros–Shklovskii (ES) variable range hopping [267] of the form

$$R_S(T) = R_0 e^{\sqrt{T_0/T}}, \tag{5.3}$$

where T_0 and R_0 are fitting parameters. In order to see that, in Fig. 5.8a we plot R_S versus $T^{-1/2}$ on a logarithmic scale. We see the ES-dependence develop from -5 V onward. The fitting parameters T_0 and R_0 are given in Fig. 5.8b. Similar dependen-

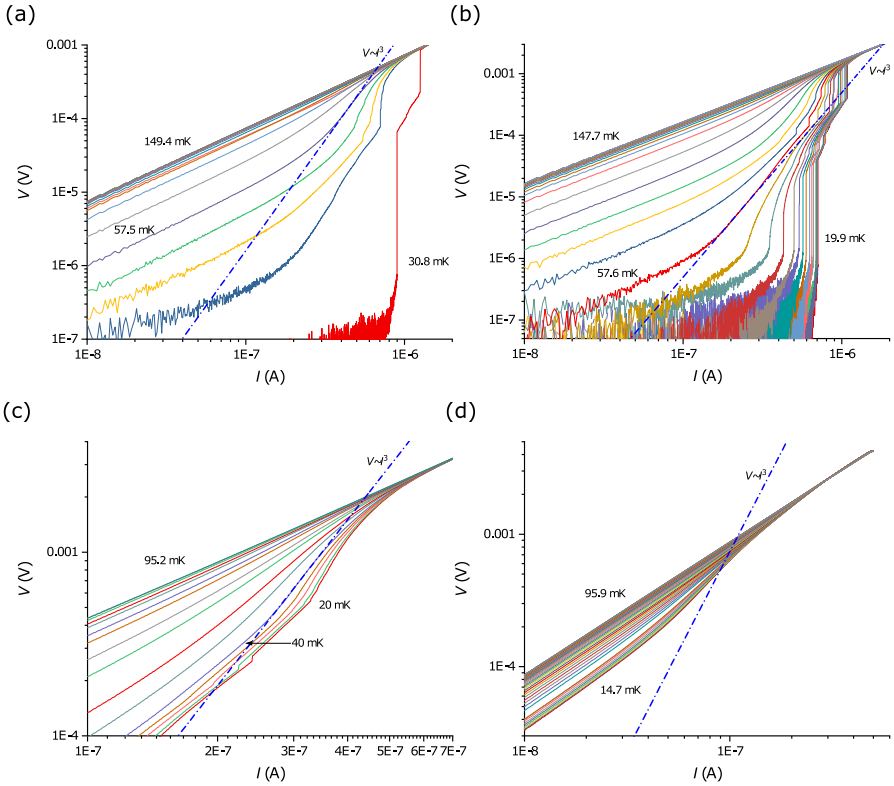

Figure 5.7: $I(V)$ characteristics taken on LGAO/GLTAO/STO at (a) 40 V, (b) 20 V, (c) 5 V and (d) 0 V. The dashed lines show the $V \propto I^3$ behavior used to determine the Berezinskii-Kosterlitz-Thouless temperature T_{BKT} correspondingly.

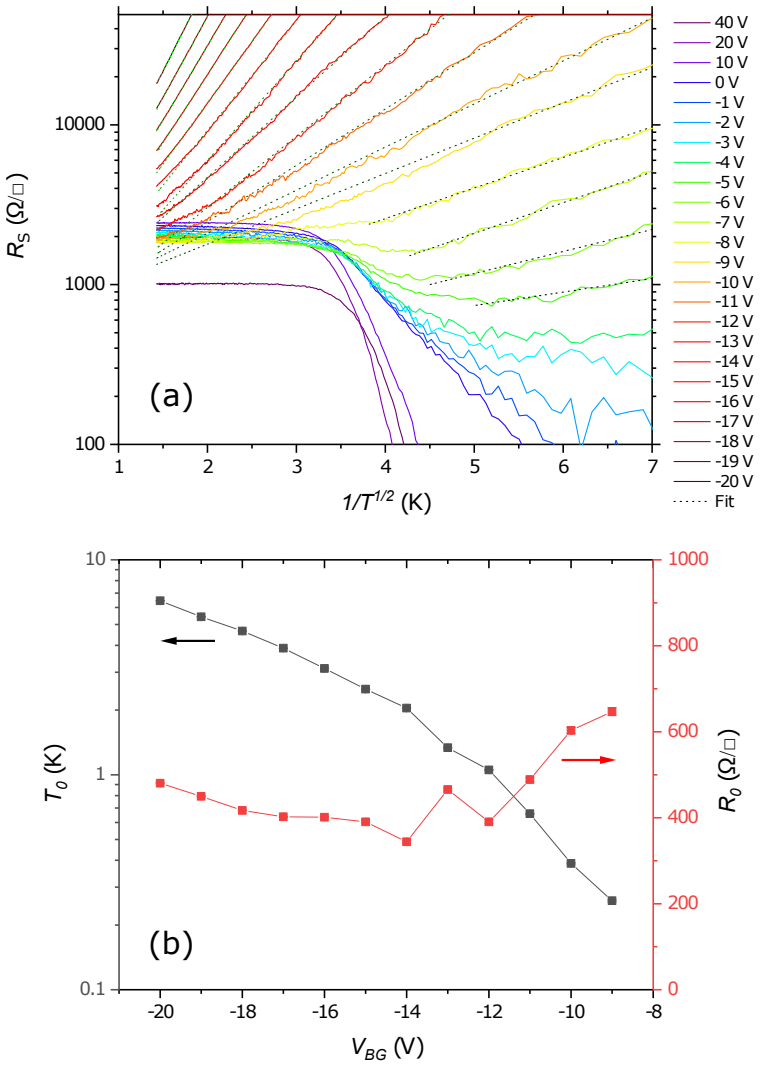

Figure 5.8: (a) Resistance versus $T^{-1/2}$ for LGAO/GLTAO/STO at different gate voltages. The dashed lines are used to fit variable range hopping behavior (see text). (b) Variation of the fit parameters of Eq. 5.1 with applied gate voltage V_{BG}.

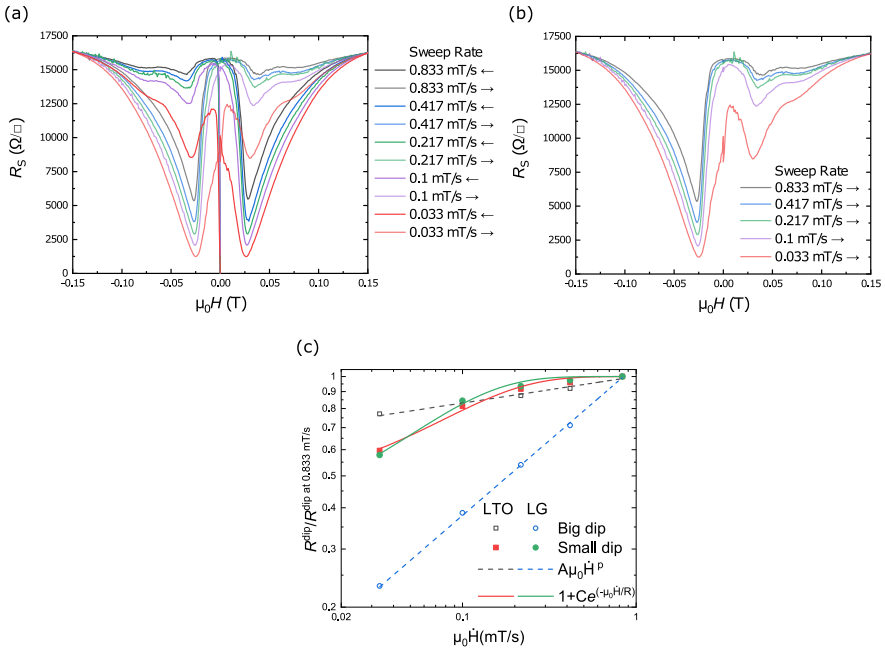

Figure 5.9: Magnetoresistance in LGAO/GLTAO/STO at a gate voltage of 30 V and at 25 mK for different magnetic field sweep rates in (a) both directions and (b) in one direction. (c) Sweep rate dependence of normalized dips and corresponding fits for LGAO/GLTAO/STO (denoted LG in the legend) and a-LTO/STO (denoted LTO in the legend).

cies have been reported for many systems exhibiting SIT, among them HTC's [268], metal films [266, 269], and superconductor-semiconductor arrays [270]. As can be seen in Fig. 5.8b, the prefactor R_0 varies with the gate voltage in a similar manner as Pb and Al films, where the prefactor depends on thickness [266]. One note to make is that, although we found that a function with power 1/2 in the exponent describes our data best, we cannot fully exclude a 1/3 dependence, which is expected for Variable Range Hopping in two dimensions. Moreover, we were not able to observe activated behavior, which may appear at even lower gate voltages, but there the sample became too insulating to measure in our setup's temperature range.

In the magnetic field dependence of the resistance (see Fig. 5.9a,b), we observe butterfly-type hysteresis in the superconducting regime, again as in a-LTO/STO. Furthermore, the hysteresis is sensitive to the field sweep rate, and the rate dependence of the dips can be fitted with Eqs. 5.1, 5.2. By driving LGAO/GLTAO/STO

through the SIT (which could not be done in a-LTO/STO) we observed a change of hysteresis (Fig. 5.10a) somewhat similar to Ref. [74]. There is no significant change between -2 V and -6 V, but at -8 V, where the local minimum on the R_S(T) curve vanishes, a crossover occurs to a different type of behavior, where the resistance of the back sweep in the positive quadrant lies above the up sweep. We should point out here that it is significant that hysteresis also and still can be observed in the insulating state at -11 V. Figs. 5.10b,c show the temperature dependence of this effect at -8 V and -11 V. At -8 V, hysteresis is already visible at 100 mK, which corresponds to T_c in the metallic state, even though R_S at that gate voltage does not show a dip anymore. Also at -11 V, hysteresis sets in at 100 mK. The observations clearly point to a state in which superconducting puddles or granules exist with a T_c of the metallic state, but where phase coherence has been lost.

One more often observed feature of the *MR* curves is a strong relaxation of the resistance when applying the field for the first time. This is seen as sharp spikes in Fig. 5.10 where the resistance increases (decreases) on the superconducting (insulating) side of the SIT. Such transient decrease near zero field was previously reported by Ref. [258], who argued that the relaxation effect of the magnetization in the sample leads to such behavior, but we observed the effect only during the initial sweep away from 0 T and not following ones. The behavior can be a sign of the magnetocaloric effect. On the other hand, developing percolation paths made of weak links, which are destroyed by a magnetic field, also can lead to such effects, especially since our samples have relatively low critical fields in the superconducting state. As we showed previously for such inhomogeneous sample measured in the VDP geometry, an increase of resistance with cooling can occur when some regions in the sample undergo a superconducting transition, but their contribution to the measured voltage yields an increase of voltage instead of decrease [230](also see Chapter 4). The application of the external magnetic field destroys these regions, and the resistance will decrease or increase depending on the distribution of the weak links.

5.3.2. Discussion

We already discussed the a-LTO/STO behavior, and the differences in magnetotransport properties between that system and LGAO/GLTAO/STO are likely to originate from a different type of disorder. In contrast to amorphous LTO/STO, LGAO/GLTAO/STO is crystalline, but strongly intermixed. In LGAO/GLTAO/STO the magnetic ions such as Gd^{3+} with 7 f-electrons and Ti^{3+} with 1 d-electron are brought to be right at the interface and in particular the Ti^{3+} distribution is in-

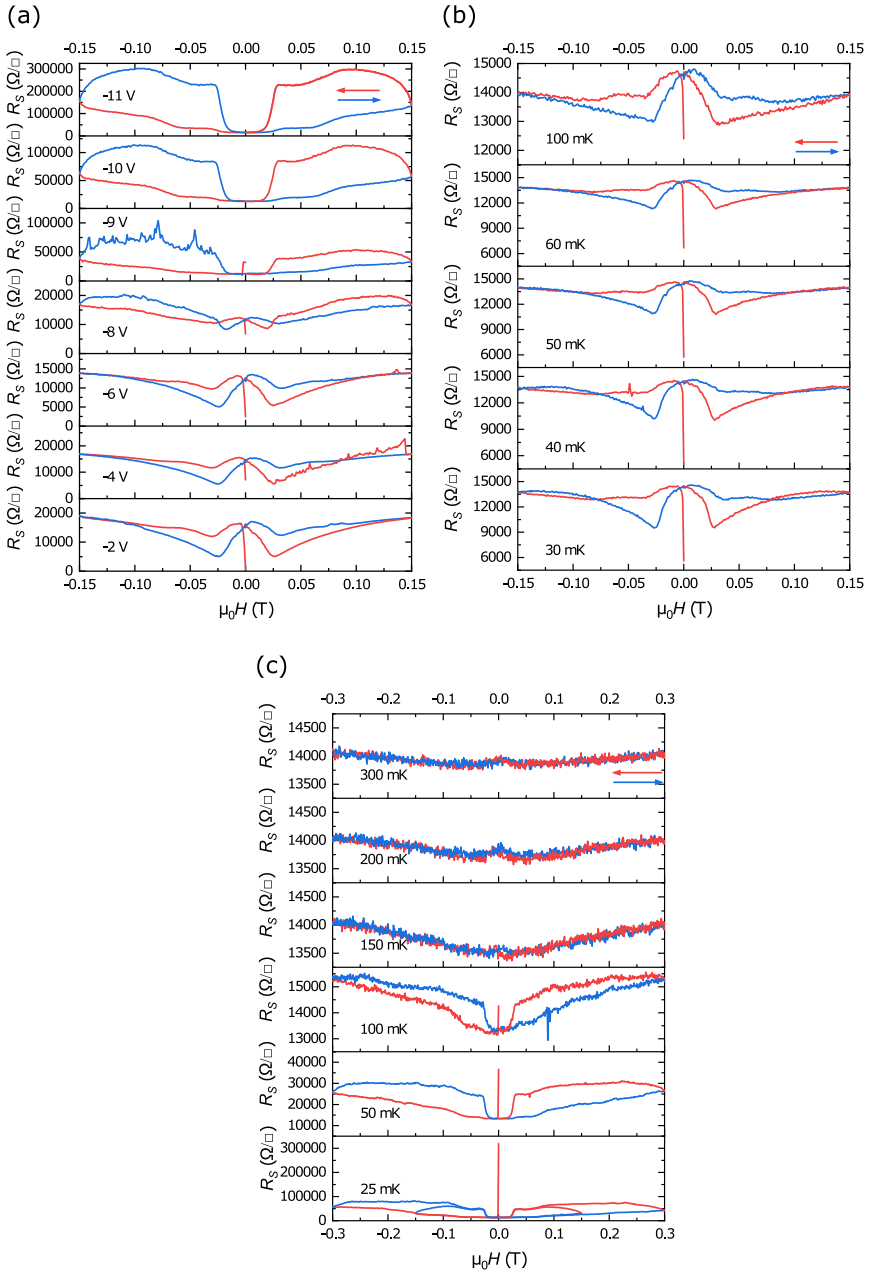

Figure 5.10: (a) Magnetoresistance *MR* for LGAO/GLTAO/STO at different gate voltages across the Superconductor-Insulator Transition (SIT) and 25 mK with a sweep rate of 0.033 T/s. (b) *MR* at various temperatures at −8 V with a sweep rate of 0.833 T/s and (c) at -11 V with sweep rate 0.033 T/s.

homogeneous. Magnetic doping suppresses the development of superconducting regions and Josephson coupling between them and, overall, leads to the lower T_c and T_{BKT} we observe. Nevertheless, this system exhibit a SIT very similar to that of granular superconductors, and many properties of this system can be understood via two-level model [257, 260] similar to case of a-LTO/STO, but the signatures of such behaviour in in the SIT is more pronounced. Moreover, driving system into insulating state in LGAO/GLTAO/STO requires smaller gate voltage range. This is in agreement with previous reports on Josephson coupling between superconducting islands in crystalline (but non-magnetic) STO-based structures [58, 60–62, 64].

The presence of magnetic doping and tunable AHE at normal state (see Chapter 3) point out that the magnetic origin of hysteresys in LGAO/GLTAO/STO can be possible. However, if we compare LGAO/GLTAO/STO with another magnetically doped interface LAO/ETO/STO, which also show tunable AHE [132], we found significant difference in their behaviour. In LAO/ETO/STO, hysteresis disappears on the Kondo-like insulating side, which is set in at voltage above SIT [132]. Moreover, the shape of hysteresis is different, and, in contrast to the LGAO/GLTAO/STO mentioned above, there is no sweep rate dependence of *MR* in LAO/ETO/STO. Still, a non-uniform magnetic state of GLTAO layer can give rise of some features of hysteresis; this non-uniform magnetic doping can enhance vortex formation as well as flux pinning at LGAO/GLTAO/STO in a somewhat similar manner to superconducting PbBi with Ni wires on top [271].

At the same time a similar behaviour of hysteresis in a-LTO/STO is indicated on the granular superconductivity as the main source of hysteresis. Indeed, the hysteresis has a characteristic butterfly shape and develops below onset of superconductivity with lowering temperature. Furthermore, the sweep rate dependents of the *MR* peaks can be fitted with the same functions as in a-LTO/STO. As we mentioned above the sweep rate dependence can be signatures of magnetocaloric effect, but the shape of hysteresis is ferromagnetic one [81, 82, 95, 258] only in insulating side of SIT.

5.4. Summary

To summarize, we have studied the occurrence of Superconductor-Insulator transitions in an amophous oxide interface system, a-LTO/STO, and in a crystalline one, LGAO/GLTAO/STO. We have observed that both systems exhibit granular behavior, but the behavior across the SIT is different due to different types of disorder. Both systems exhibit hysteresis below T_c, and although previously

similar hysteresis was argued to be due to the presence of (coexistent) ferromagnetism, we propose it is rather the signature of granularity in the superconducting systems. a-LTO/STO shows the presence of large scale non-uniformities, and a complex response to magnetic field sweeps which points to varying stregth of superconducting area's and the links between them. LGAO/GLTAO/STO also shows properties of typical granular superconducting material, and can be better described by the two-level model in a simplified picture. The magnetic moments in LGAO/GLTAO/STO seem to suppress the formation of the weak links between grains to the lower temperature and alter properties of this system compare to LAO/STO. Moreover, we observed ES-like temperature dependence of resistance on the insulating side of transition.